IEEE Access
Multidisciplinary | Rapid Review | Open Access Journal

SPECIAL SECTION ON EMERGING TECHNOLOGIES FOR ENERGY INTERNET

Received February 29, 2020, accepted March 11, 2020, date of publication March 16, 2020, date of current version March 25, 2020.

Digital Object Identifier 10.1109/ACCESS.2020.2980860

An Improved Finite Control Set-MPC-Based Power Sharing Control Strategy for Islanded AC Microgrids

TIANHAO CHEN[1,2,3], (Student Member, IEEE), OMAR ABDEL-RAHIM[1,4], (Senior Member, IEEE), FAXIANG PENG[1], (Student Member, IEEE), AND HAOYU WANG[1], (Senior Member, IEEE)

[1]School of Information Science and Technology, ShanghaiTech University, Shanghai 201210, China
[2]Shanghai Institute of Microsystem and Information Technology, Chinese Academy of Sciences, Shanghai 200050, China
[3]University of Chinese Academy of Sciences, Beijing 100049, China
[4]Aswan Power Electronic Application Research Center (APEARC), Faculty of Engineering, Aswan University, Aswan 81542, Egypt

Corresponding author: Haoyu Wang (wanghy.shanghaitech@gmail.com)

This work was supported by the National Natural Science Foundation of China under Grant 51607113.

ABSTRACT Hierarchical linear control scheme is widely used in ac microgrids. However, its transient response is slow and parameter tuning is time-consuming. Finite Control Set-Model Predictive Control (FCS-MPC) strategy has desired dynamic performance. Nevertheless, it requires an additional sensor to measure the inductor current. This article aims to mitigate these problems by introducing an improved FCS-MPC strategy for paralleled Voltage Source Inverters (VSIs). A capacitor current estimator is employed to reduce the extra current sensor in each VSI. The proposed control scheme consists of two loops: voltage reference generation loop and voltage tracking loop. The voltage reference generation loop achieves accurate load power sharing using virtual impedance-based droop control. Thus, communication is unnecessary among parallel VSIs. The voltage tracking loop utilizes a modified FCS-MPC block with capacitor current estimator to regulate the VSI output voltage. In order to verify the concept of the proposed control strategy, an ac microgrid consisting of two paralleled VSIs is implemented in dSPACE DS1202 hardware-in-the-loop platform. Then a single VSI hardware prototype is implemented and tested experimentally. The proposed method has the merits of good extensibility, low system cost and compact structure. Its steady-state performance is competitive with hierarchical linear control, while the transient response is significantly improved.

INDEX TERMS AC microgrids, current estimator, finite control set, model predictive control, and power sharing control.

I. INTRODUCTION

Microgrid is an emerging technology for energy distribution systems due to its compatibility with renewable energies [1]–[3]. By locally integrating multiple distributed generations (DGs), they can achieve higher robustness and flexibility than individual sources [4]–[6]. The ac microgrid can operate in both grid-connected and islanded modes. In islanded mode, in order to ensure stable and economic operation of the microgrid, the real and reactive powers of DGs should be split in proportion to their power rating [7].

Droop control can realize the power sharing control without external communications among different voltage source inverters (VSIs) [8]–[13]. Conventionally, overall decentralized control structure in microgrids is based on hierarchical linear control with two loops: outer loop droop control and inner loop voltage/current feedback control. Due to its significance, a lot of researches have been done in the literature to improve the overall system performance under this architecture [8]–[11]. In [9], a power derivative term is added into conventional droop. It helps to improve the transient response in power sharing between inverters. In [10], [11], adaptive virtual impedance is proposed to improve the accuracy of reactive power sharing with nonlinear loads. In [12], by combining the virtual impedance and conventional droop control, the load powers can be shared with mismatched line impedances. In [13], a universal droop control scheme for different types of output impedance is proposed. It can be

The associate editor coordinating the review of this manuscript and approving it for publication was Huiqing Wen.

applied to all practical inverters without the information of the impedance angle. In [14], a fully distributed hierarchical control strategy is proposed. It integrates the secondary control and tertiary control into a single control level. Instead of average models, detailed switching models are employed. However, hierarchical linear control is inherently slow since the bandwidth of the outer loop is much smaller than the inner loop [15]. Moreover, the effectiveness of the droop control may be deteriorated by incorporating cascade linear control [16]. With its fast transient characteristics, the model predictive control (MPC) strategy emerges as a candidate solution.

In contrast to linear control, finite control set-MPC (FCS-MPC) is based on a fundamentally different principle [17], [18]. Instead of designing loops for each controlled variable independently and then cascading them together, FCS-MPC uses the mathematical model of VSI to predict its future behavior and then determines the optimal switching state of the power converter according to a specified cost function. In [19], a typical FCS-MPC scheme for LC-filterer VSI is introduced. It has merits of robustness, excellent transient characteristics and easiness to include nonlinearities, constraints, and additional control objectives. Hence, the FCS-MPC principle has emerged as an attractive candidate for the control of VSIs [20]–[25]. In [20], current sensorless MPC control is proposed to reduce the hardware budget and to enhance system reliability. References [21]–[23] discuss the applications of multistep MPC, revealing that increasing the length of predictive horizon improves performance at the cost of higher computational burden. In [26], a secondary control scheme for voltage and frequency restoration is proposed. It incorporates predictive mechanisms into distributed generations.

To the best of authors' knowledge, research work on MPC in the coordinated control of paralleled inverters in microgrids is still immature. In [27], a multiple-input-multiple-output state-space model to control paralleled system is presented. It achieves good performance on both voltage-reference tracking and current sharing objectives. In [28], a centralized control system that coordinates parallel operations of different VSIs within a microgrid is presented. However, both of them require a centralized controller or require external communication between controllers. In [29], [30], a cost function is employed to realize multiple control objectives and to select the optimal switching state. However, all of these strategies require an extra measurement of inductor current to predict the state variable in the next sampling time. This leads to increased hardware budget and power loss.

This article presents a new control scheme based on FCS-MPC strategy for islanded ac microgrids. Droop control with virtual impedance is used to generate reference voltage for the inner loop and to realize load power sharing. An improved FCS-MPC strategy is adopted to track the voltage reference and to select optimal control action at the next step. The proposed method can achieve comparable steady-state performance with hierarchical linear control, while its transient response is significantly improved. Compared to existing MPC based schemes, system budget is reduced. Moreover, the physical limitations of sensors such as vulnerable to the noise, limited lifespan can be overcome.

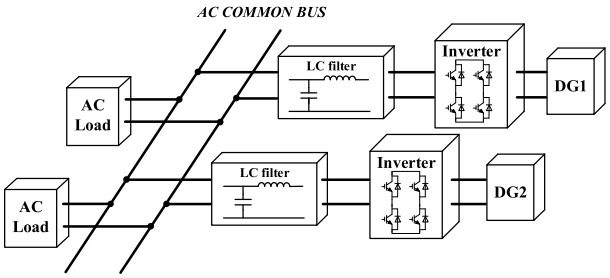

FIGURE 1. Diagram of a VSI enabled ac microgrid.

The remaining sections of the article are organized as follows: Section II, the structure of the ac microgrid is described. Section III provides basic model of LC-filtered VSI. In Section IV, a modified algorithm that reconstructs the state variable and the design of current estimator is presented. Section V describes building an ac microgrid from FCS-MPC regulated VSIs. Real-time hardware-in-the-loop (HIL) results and the experimental verification are given in Section VI. Finally, Section VII gives the conclusion.

II. SYSTEM DESCRIPTION

Fig. 1 depicts a simple ac microgrid. It consists of two DG units connected through VSI in parallel. Since the DGs are usually connected to the energy storage system (ESS) to ensure a stable supply system, we assume that the inputs of distributed inverters are dc power sources [30]. The load power is shared through an AC common bus. Such microgrid can be connected to the main grid or operates in islanded mode. In latter mode, droop control is widely used to ensure the accurate power sharing among different modules due to its decentralized feature [1].

Fig. 2 shows the conventional hierarchical linear control in ac microgrids. Droop control functions in the outer loop to regulate the capacitor voltage amplitude and frequency of output voltage. In such hierarchical structure, droop control works as voltage reference generator for the inner cascade linear control loop. These voltage/current loops are designed independently. As a result, the bandwidth of the outer loop needs to be an order of magnitude smaller than the inner one, which gives rise to slow transient performance. To solve this problem, FCS-MPC strategy is employed to improve the tracking performance due to its excellent transient performance.

A combination of the droop control loop with the traditional FCS-MPC scheme is shown in Fig. 4. It is noticed that besides the capacitor voltage v_c and output current i_o, the measurement of inductor current i_f is also needed to predict the voltage in the next sampling time. To overcome this limitation, the model of single-phase inverter needs to be reconstructed.

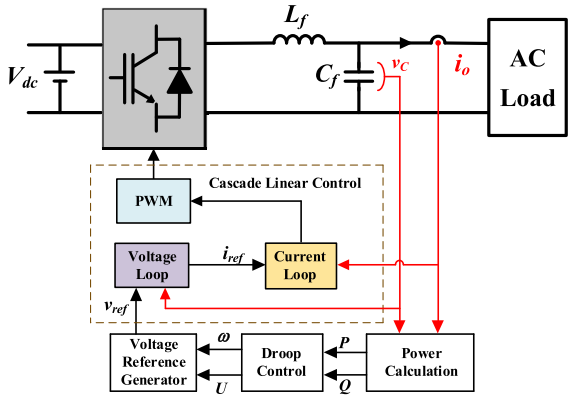

FIGURE 2. Conventional hierarchical linear control in ac microgrid.

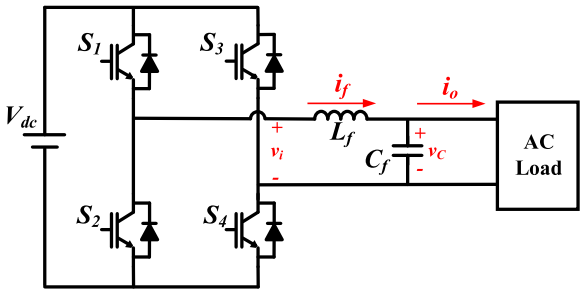

FIGURE 3. Schematic of single-phase LC-filtered VSI.

III. MPC FOR LC-FILTERED VSI

An MPC strategy relies on the mathematical model of system to predict how the possible control actions would affect system response. Consequently, the action that is expected to minimize a certain cost function is applied and the process is sequentially repeated.

In order to achieve a good control performance when deploying such technique to VSI, proper models of both the converter and filter are needed. In particular, single-phase VSI shown in Fig. 3 is the commonly used converter topology in ac microgrids. It can be seen that an LC filter, which attenuates the switching harmonics is connected at the output of VSI.

A. MODEL OF LC-FILTERED VSI

FCS-MPC predicts the future behavior of the state variable by enumerating all possible control action. As a result, the dynamic system model is needed. According to Kirchhoff laws, the LC filter, as shown in Fig. 3, can be modeled as

$$\begin{cases} L_f \dfrac{di_f}{dt} = v_i - v_c \\ C_f \dfrac{dv_c}{dt} = i_f - i_o \end{cases} \tag{1}$$

where L_f and C_f are filter inductance and capacitance. v_i, v_c, i_f, i_o are inverter voltage vector, capacitor voltage, inductor current and load current, respectively. The continuous-time state-space form of (1) can be rewritten as

$$\frac{d}{dt}\begin{bmatrix} i_f \\ v_c \end{bmatrix} = A\begin{bmatrix} i_f \\ v_c \end{bmatrix} + B\begin{bmatrix} i_o \\ v_i \end{bmatrix} \tag{2}$$

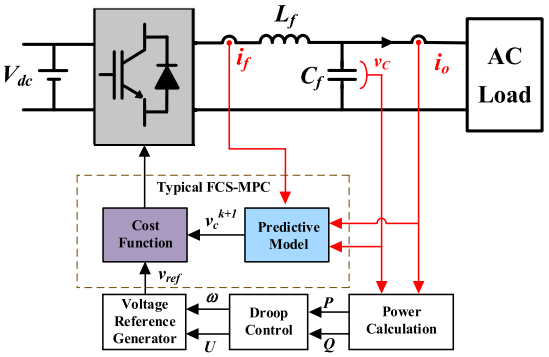

FIGURE 4. Typical FCS-MPC based control scheme in ac microgrid.

TABLE 1. Switch states for single-phase full-bridge inverter.

State	Switch State	Voltage Vector v_i
S_1 and S_4 are on and S_2 and S_3 are off	10	V_{dc}
S_2 and S_3 are on and S_1 and S_4 are off	01	$-V_{dc}$
S_1 and S_3 are on and S_2 and S_4 are off	11	0
S_2 and S_4 are on and S_1 and S_3 are off	00	0

* Switch state is 1 if an upper switch is on and 0 if a lower switch is on.

where

$$A = \begin{bmatrix} 0 & -\dfrac{1}{L_f} \\ \dfrac{1}{C_f} & 0 \end{bmatrix} \tag{3}$$

and

$$B = \begin{bmatrix} 0 & \dfrac{1}{L_f} \\ -\dfrac{1}{C_f} & 0 \end{bmatrix} \tag{4}$$

The equations above take v_c and i_f as state variables and the voltage vector v_i and output current i_o as control variables. The voltage vectors of single-phase full bridge inverter are shown in Table 1. The full-bridge consists of two legs. Each leg has two switches: one upper and one lower. To avoid a short circuit, they cannot conduct simultaneously. Therefore, the switch state is defined as 1 when the upper switch is on and the lower switch is off. On the contrary, if the lower switch is on and the upper switch is off, the switch state is 0. V_{dc} is the dc input voltage.

B. MODEL DISCRETIZATION

In order to implement the model developed in the previous section, a discrete-time model of the filter can be obtained from (4). By utilizing a zero-order hold approach, the equation is derived as [19], [21]

$$\begin{bmatrix} i_f(k+1) \\ v_c(k+1) \end{bmatrix} = A_d\begin{bmatrix} i_f(k) \\ v_c(k) \end{bmatrix} + B_d\begin{bmatrix} i_o(k) \\ v_i(k) \end{bmatrix} \tag{5}$$

with

$$A_d = e^{AT_s} = \begin{bmatrix} \cos(\omega_0 T_s) & -\frac{C_f}{\omega_0}\sin(\omega_0 T_s) \\ \frac{L_f}{\omega_0}\sin(\omega_0 T_s) & \cos(\omega_0 T_s) \end{bmatrix} \quad (6)$$

and

$$B_d = \int_0^{T_s} e^{A\tau} B d\tau = \begin{bmatrix} 1-\cos(\omega_0 T_s) & \frac{C_f}{\omega_0}\sin(\omega_0 T_s) \\ -\frac{L_f}{\omega_0}\sin(\omega_0 T_s) & 1-\cos(\omega_0 T_s) \end{bmatrix} \quad (7)$$

where $v_c(k+1)$ and $i_f(k+1)$ are the predicted capacitor voltage and inductor current at $(k+1)^{th}$ instant. T_s is the sampling time and ω_0 is the resonant frequency of LC filter.

C. COST FUNCTION

As the capacitor voltage at the $(k+1)^{th}$ instant, $v_c(k+1)$, is predicted according to equation (5), the next step is to design the cost function to select the optimal voltage vector. One important merit of FCS-MPC is its flexibility to achieve multiple objectives control and to include constraints and other requirements in a simple way [24], [31]. To facilitate the design, the simplest cost function to minimize the voltage error is chosen as

$$g = (v_{ref} - v_c(k+1))^2 \quad (8)$$

where v_{ref} is the reference voltage generated by the outer droop control loop.

D. TWO-STEP PREDICTION

The operation principle of predictive voltage control is graphically illustrated in Fig. 6. Ideally, the calculation of predictive value takes negligible time, as shown in Fig. 6(a). The capacitor voltage at k^{th} instant $v_c(k)$ is measured at t_k, and the optimal voltage vector is immediately calculated. Consequently, the switching state that minimizes the cost function (8) at $(k+1)^{th}$ instant is selected and applied at time t_k.

However, practically when the control FCS-MPC based control scheme is experimentally implemented, the calculation time is no longer negligible compared with the sampling time [32]. As shown in Fig. 6(b), there is a delay between the instant when the voltages are measured and the instant of actuation of the new switching state, as shown in Fig. 6(b). During this interval, the previous switching state keeps to be valid. For instance, the selected voltage vector considering measurements at k^{th} instant is actually updated near time t_{k+1}. This makes the capacitor voltage deviate from the reference. When the outer droop loop is introduced as a voltage reference generator to realize power sharing, the computational burden is further increased and the delay effect is aggravated. Consequently, the capacitor voltage will fluctuate around its reference. This incurs the voltage oscillation.

Two-step prediction principle is a simple but effective solution to compensate for this delay. Its operation principle is illustrated, as shown in Fig. 6(c). At k^{th} instant, the prediction of voltage in $(k+2)^{th}$ instant is calculated and the optimal voltage vector is selected, while the switching state applied at k^{th} instant is selected at the previous step. Therefore, this two-step prediction obviates the calculation delay and applies the switching state selected at the previous step. Correspondingly, the prediction of the state variables at the $(k+1)^{th}$ instant considering the switching states applied at t_k, which is selected at t_{k-1}, can be expressed as

$$\begin{bmatrix} i_f(k+1) \\ v_c(k+1) \end{bmatrix} = A_d \begin{bmatrix} i_f(k) \\ v_c(k) \end{bmatrix} + B_d \begin{bmatrix} i_o(k) \\ v_i(k) \end{bmatrix} \quad (9)$$

where $v_i(k)$ is the optimal voltage vector calculated in the previous step. $i_f(k+1)$ and $v_c(k+1)$ are predicted inductor current and capacitor voltage at the $(k+1)^{th}$, respectively.

Moreover, the prediction of the capacitor voltage for the next sampling instant $(k+2)^{th}$ for all possible switching states are derived as

$$\begin{bmatrix} i_f(k+2) \\ v_c(k+2) \end{bmatrix} = A_d \begin{bmatrix} i_f(k+1) \\ v_c(k+1) \end{bmatrix} + B_d \begin{bmatrix} i_o(k+1) \\ v_i(k+1) \end{bmatrix} \quad (10)$$

where $v_i(k+1)$ is the candidate voltage vector to be evaluated. $i_f(k+2)$ and $v_c(k+2)$ are predicted inductor current and capacitor voltage at the $(k+2)^{th}$, respectively. Since the sampling time is chosen to be much smaller than the load dynamics, the load current can be assumed as constant during one sampling period. Thus, $i_o(k+1)$ in (10) can be replaced by $i_o(k)$ [19]. Hence, $v_c(k+2)$ is fed into cost function (8) instead of $v_c(k+1)$ for delay compensation.

IV. PROPOSED CONTROL SCHEME

Apart from the measurement of v_c and i_o, extra measurement of the inductor current is required to predict the future behavior of voltage in equation (10), compared to the conventional linear control. Although the FCS-MPC based control scheme for microgrids has better dynamic performance, it also increases the hardware cost and the computational burden. To avoid this shortcoming but still retain the merits of FSC-MPC, an improved control scheme is proposed as shown in Fig. 5. A two-step prediction technique is employed to calculate the delay compensation. Moreover, the model is reconstructed and a current observer is designed to predict the future behavior of capacitor voltage $v_c(k+2)$ without the information of inductor current.

A. RECONSTRUCTION OF TYPICAL MODEL

From equation (5), we could rewrite the expression of $v_c(k+1)$ as

$$v_c(k+1) = \cos(\omega_0 T_s)v_c(k) + (1-\cos(\omega_0 T_s))v_i(k) + \frac{L_f}{\omega_0}\sin(\omega_0 T_s)i_f(k) - \frac{L_f}{\omega_0}\sin(\omega_0 T_s)i_o(k) \quad (11)$$

It is noticeable from (11) that the absolute values of coefficients of $i_f(k)$ and $i_o(k)$ are equal and $i_f(k) - i_o(k)$ happens to be the capacitor current i_c.

Hence, to avoid the measurement of the inductor current i_f, we need to reconstruct the dynamic model and define i_c as

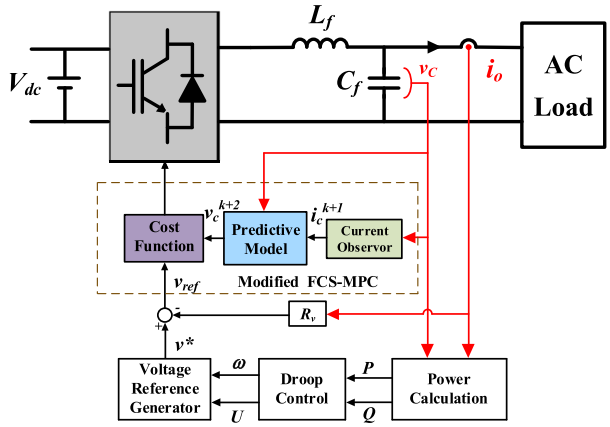

FIGURE 5. Proposed enhanced control scheme in ac microgrid.

a new state variable. The upcoming analysis is based on the assumption that the load current i_o is not varying during one sampling period.

$$\frac{di_0}{dt} = 0 \tag{12}$$

Dynamic model (1) can be reconstructed as

$$\begin{cases} L_f \dfrac{di_c}{dt} = L_f\left(\dfrac{di_f}{dt} - \dfrac{di_0}{dt}\right) = v_i - v_c \\ C_f \dfrac{dv_c}{dt} = i_c \end{cases} \tag{13}$$

In the reconstructed dynamic model (13), the state variable inductor current in the dynamic model (1) is converted to be the capacitor current. In the next section, we design a current estimator for i_c based on the relationship between capacitor voltage and current.

B. DESIGN OF FULL-ORDER ESTIMATOR

A full-order observer for the system can be used to estimate the state vector. An observer is an open-loop model of the system which includes a correcting term based on the measured output, which is expressed as

$$\begin{cases} \dfrac{d\hat{i}_c}{dt} = \dfrac{1}{L_f}(v_i - \hat{v}_c) + k_1(v_c - \hat{v}_c) \\ \dfrac{d\hat{v}_c}{dt} = \dfrac{1}{C_f}\hat{v}_c + k_2(i_c - \hat{i}_c) \end{cases} \tag{14}$$

where k_1, k_2 are the observer gains. Implementing the full-ordered observer (14) in discrete-time controller with sampling and command updates at intervals T_s, we can obtain the estimation of i_c at the next sampling instant by using the forward Euler method

$$\hat{i}_c(k+1) = \hat{i}_c(k) + T_s \begin{bmatrix} \dfrac{1}{L_f}\left(v_i(k) - \hat{v}_c(k)\right) \\ +k_e\left(v_c(k) - \hat{v}_c(k)\right) \end{bmatrix} \tag{15}$$

where $\hat{i}_c(k+1)$ represents the estimated capacitor current, $v_i(k)$ is the optimal voltage vector calculated at the previous step. and k_e is the observer gain. The observer gain k_e can be designed using the pole assignment strategy [19], [33].

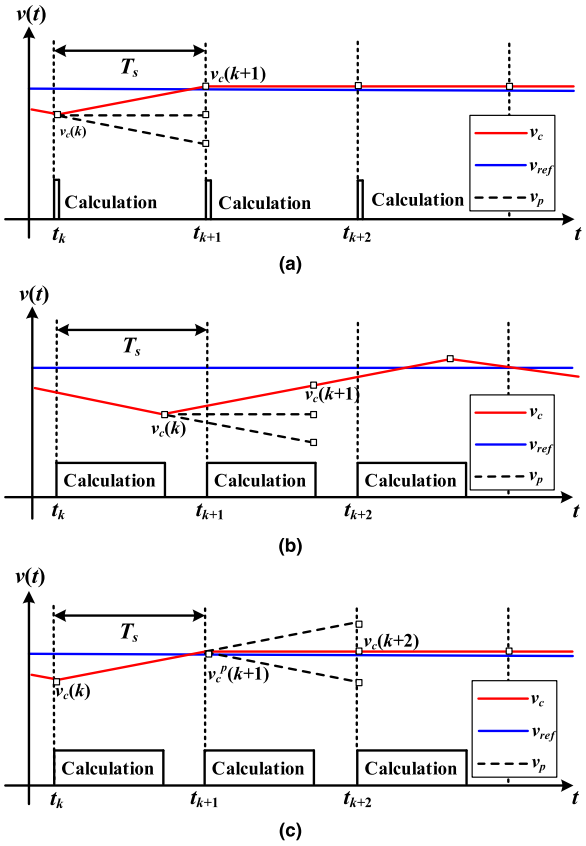

FIGURE 6. Operation of the predictive voltage control. (a) Without delay (ideal case). (b) With delay and one-step prediction (practical case). (c) With delay and two-step prediction (practical case).

In [34], simple design procedure for the full-order estimator gains' selection is introduced. To guarantee the stability of the estimator, the poles (i.e., eigenvalues) of (15) has to be set inside the unit circle of the z-plane.

C. IMPLEMENTATION OF MODIFIED FCS-MPC

To compensate for the delay in actuation, the principle of two-step FCS-MPC is presented in the previous section. Based on equation (10), the prediction of $v_c(k+2)$ need the information of $i_f(k+1)$. According to estimator (15), the estimation of capacitor current for $(k+1)^{th}$ instant $\hat{i}_c(k+1)$ is obtained. Inherently, $i_f(k+1)$, in (10), can be replaced by the result of the current estimator (15), where the estimation of $\hat{v}_c(k)$ can be replaced by $v_c(k+1)$ calculated at k^{th} instant. As a result, the modified FCS-MPC combined with the current observer is expressed as

$$\begin{aligned} v_c(k+2) = {} & \cos(\omega_0 T_s)v_c(k+1) \\ & +(1-\cos(\omega_0 T_s))v_i(k+1) \\ & +\frac{L_f}{\omega_0}\sin(\omega_0 T_s)\hat{i}_c(k+1) \end{aligned} \tag{16}$$

$$\begin{aligned} v_c(k+1) = {} & \cos(\omega_0 T_s)v_c(k) \\ & +(1-\cos(\omega_0 T_s))v_i(k) + \frac{L_f}{\omega_0}\sin(\omega_0 T_s)\hat{i}_c(k) \end{aligned} \tag{17}$$

where $v_i(k+1)$ is the candidate voltage vector to be evaluated.

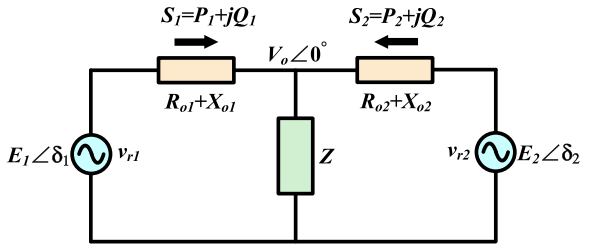

FIGURE 7. Equivalent model of the microgrid with two inverters.

The third term of (16) can be obtained from the current observer (15). In (17), $v_c(k)$ and $v_i(k)$ are the predicted voltage and selected voltage vector and in the previous step. $\hat{i}_c(k)$ is the result of the current observer in the previous step.

Finally, (16) is inserted into (8) to minimize the cost function. Then the optimal switching state is selected and actuate to the VSI. Another term v_{ref} in (8) will be generated by outer droop control, which will be introduced in next Section.

V. BUILDING AN AC MICROGRID

A. POWER SHARING IN MICROGRID

Fig. 7 shows the equivalent diagram of a two-unit microgrid. Two VSIs are connected to the ac bus through a feeder. The generic feeder impedance of each converter can be expressed as $R_{oi}+X_{oi}$, where R_{oi} and X_{oi} represent the feeder resistance and reactance. The active and reactive powers drawn from the ac bus can be expressed as [8]–[10]

$$P_i = \frac{E_i}{R_{oi}^2 + X_{oi}^2}[R_{oi}(E_i - V_0\cos\delta_i) + X_{oi}V_0\sin\delta_i] \quad (18)$$

$$Q_i = \frac{E_i}{R_{oi}^2 + X_{oi}^2}[-R_{oi}V_0\sin\delta_i + X_{oi}(E_i - V_0\cos\delta_i)] \quad (19)$$

where i is the index indicating each inverter. E_i and V_o are the amplitudes of VSI and load voltage. δ_i is the power angle.

The output impedance of the closed-loop inverter affects the power sharing accuracy and determines the droop control strategy [35], [36]. Although the closed-loop output impedance can be set to either inductive or resistive using the virtual impedance technique, it is better to shape it resistive [30]. This is because resistive impedance does not vary with frequency, and the entire frequency range is covered with a current feedback loop. In order to program a stable resistive output impedance, we can drop the output voltage reference proportionally to the output current, using the following instantaneous droop scheme

$$v_{ref} = v^* - R_v i_0 \quad (20)$$

where R_v is the resistive virtual impedance, v_{ref} is the capacitor voltage reference to be fed into cost function (8), while v^* is the voltage reference provided by the outer droop control

When the virtual resistance R_v is set high enough so that the output impedance becomes dominantly resistive, a reasonable assumption can be made that power angle δ_i is small between the voltage vectors at VSI and microgrid terminals. It can be stated that $\sin\delta_i \approx \delta_i$, $\cos\delta_i \approx 1$, and $X_{oi} \approx 0$, in (18) and (19). This leads to

$$P_i = \frac{E_i}{R_v}(E_i - V_0) \quad (21)$$

$$Q_i = -\frac{E_i V_0 \delta}{R_v} \quad (22)$$

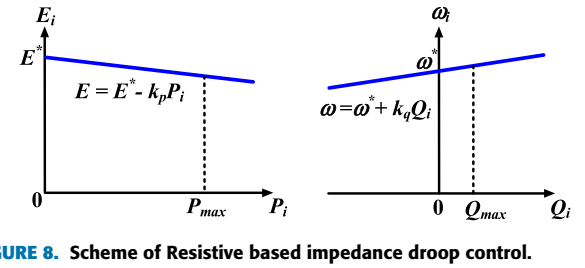

FIGURE 8. Scheme of Resistive based impedance droop control.

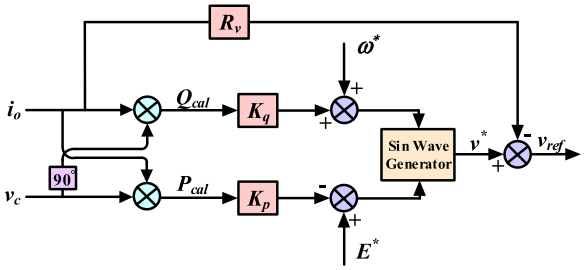

FIGURE 9. Block diagram of droop control with resistive virtual impedance.

B. DROOP CONTROL STRATEGY

$$E_i = E^* - k_p P_{cal} \quad (23)$$

$$\omega_i = \omega^* + k_q Q_{cal} \quad (24)$$

where E_i and ω_i are reference voltage amplitude and frequency used to generate v^*, which is fed to the virtual impedance loop (20), while E^* and ω^* are nominal voltage amplitude and frequency, respectively. Droop coefficients k_p and k_q, determine the slope of the droop curves and voltage drops and frequency boosts for resistive output impedance as shown in Fig. 8. Such coefficients are normally designed in proportion to the power rating of VSIs. Finally, the real and reactive powers P_{cal} and Q_{cal} are calculated and fed into equations (23) and (24). Fig. 9 shows the detailed diagram of outer power-flow control based on droop theory, where a resistive virtual impedance is added.

Conventionally, P_{cal} and Q_{cal} need to be damped through low-pass filters, which usually have an order of magnitude smaller bandwidth than underlying loops in hierarchical linear control scheme [10]. This leads to a very slow transient response. On the contrary, filtering is unnecessary if inner control is achieved by the FCS-MPC, since the speed for FCS-MPC scheme is only limited by the sampling time T_s. Furthermore, since the fluctuations in P_{cal} and Q_{cal} is damped by the droop coefficients, k_p and k_q, the normal oscillations in P_{cal} and Q_{cal} have trivial influence on the results of E and ω. Moreover, this improved FCS-MPC based control

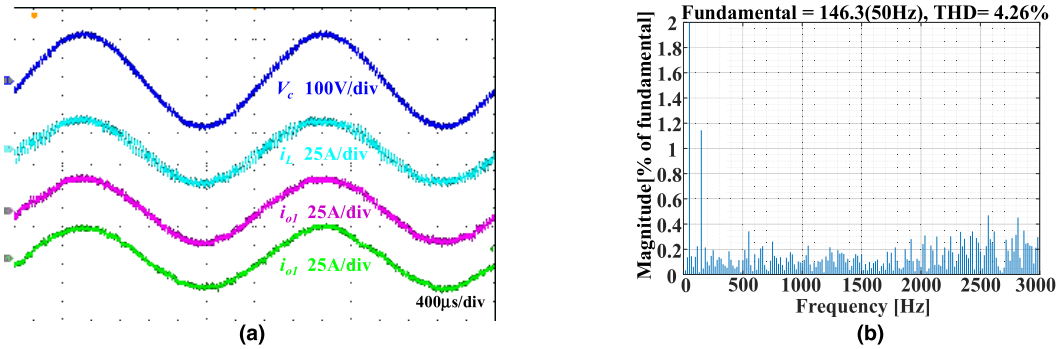

FIGURE 10. Steady-state waveforms (a) and THD (b) of typical single-step FCS-MPC.

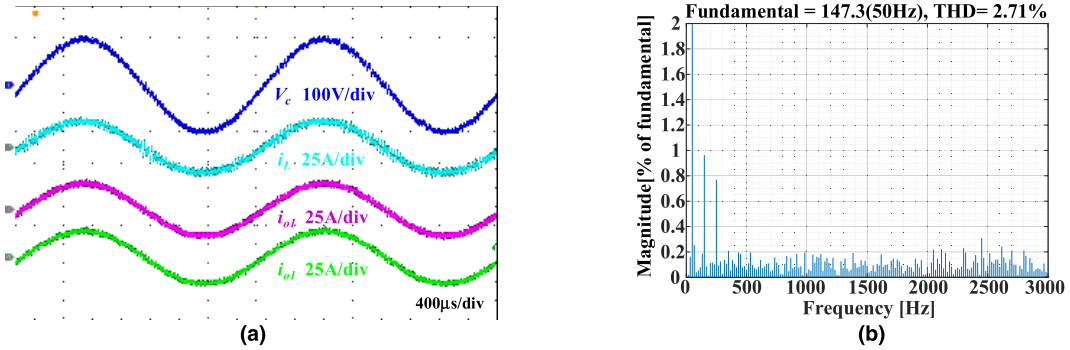

FIGURE 11. Steady-state waveforms (a) and THD (b) of proposed control scheme.

scheme can be easily combined with different variants of the cost function and advanced droop strategy. Therefore, the limitation of dynamic performance using conventional hierarchical control is eliminated.

Control strategy described in (23) and (24) is commonly referred to as the conventional droop control in the literature [8], [9], [11]. The main advantage of it lies in the fact that it is fully decentralized. However, it also has certain practical limitations, such as steady-state deviation. In [10], [14], certain modifications with secondary control have been introduced to eliminate this steady-state deviation. However, secondary control usually requires additional low bandwidth communication. This increases the implementation difficulty with a complex control. Moreover, the advantages of improved FCS-MPC over cascade linear control can be proved regardless of the specific variant of droop strategy. For simplicity consideration, the classic droop control is employed to validate the concept.

VI. RESULTS AND DISCUSSIONS

To validate the concept of the proposed control scheme, HIL simulations for an ac microgrid consisting of two parallel VSIs and experiments for one VSI system are carried out.

A. HIL VALIDATION

The ac microgrid shown in Fig. 1 is modeled and implemented in dSPACE DS1202, which is a real-time HIL simulation platform. The parameters of the test platform are listed in Table 2 . Nominal parameters and power ratings

TABLE 2. Parameter of hil test system.

Category	Parameter	Symbol	Quantity
Hierarchical linear control	Virtual Impedance	R_v	2Ω
	Switching frequency	f_{sw}	5kHz
	PI at outer voltage loop	k_p, k_i	7.5, 0.4
	PI at inner current loop	k_p, k_i	1.1, 0.1
FCS-MPC based control	Sampling time	T_s	40µs
	Gain of current estimator	k_e	12,000
Common	DC link voltage	V_{dc}	200V
	Nominal frequency	ω^*	2π*50Hz
	Nominal voltage	E^*	110V
	Line impedance	R_{line}, L_{line}	0.1Ω,3.5mH
	VSI rating	P	1.75kW
	Load Resistance	R_l	3.45Ω
	Droop coefficient	k_p, k_q	0.001, 0.0025
	LC-filter	L_f, C_f	2.3mH, 20µF

of two DGs are chosen to be identical. Droop control with resistive virtual impedance outer loop is used to generate the voltage reference. For a fair comparison, the average switching frequencies of the converters are equal for hierarchical linear method and the FCS-MPC method. To achieve this, the sampling period of FCS-MPC is chosen as 40 μs, which can obtain an average switching frequency of about 5 kHz [37].

The comparison between the steady-state performance of typical single-step FCS-MPC and modified FCS-MPC are shown in Fig. 10 and Fig. 11, respectively. It is worth mentioning that the modified strategy uses one fewer current sensor than typical MPC as demonstrated in Fig. 4 and Fig. 5. The capacitor voltage and its total harmonic distortion (THD), inductor current and load current of DG1 are pre-

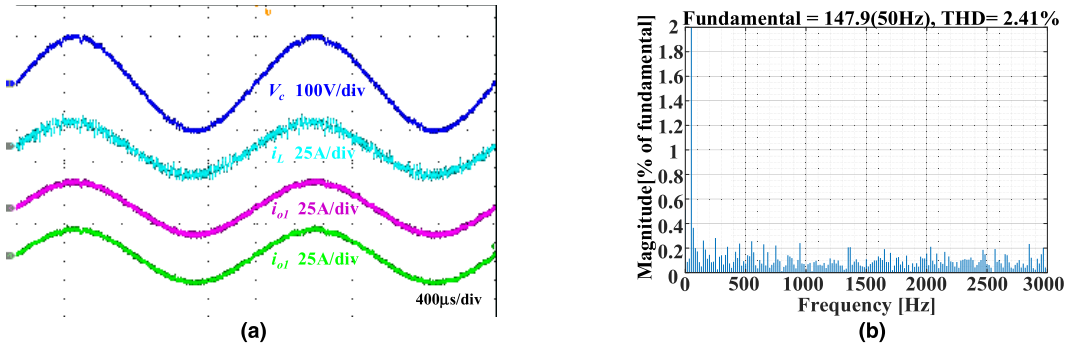

FIGURE 12. Steady-state waveforms (a) and THD (b) of two-step FCS-MPC.

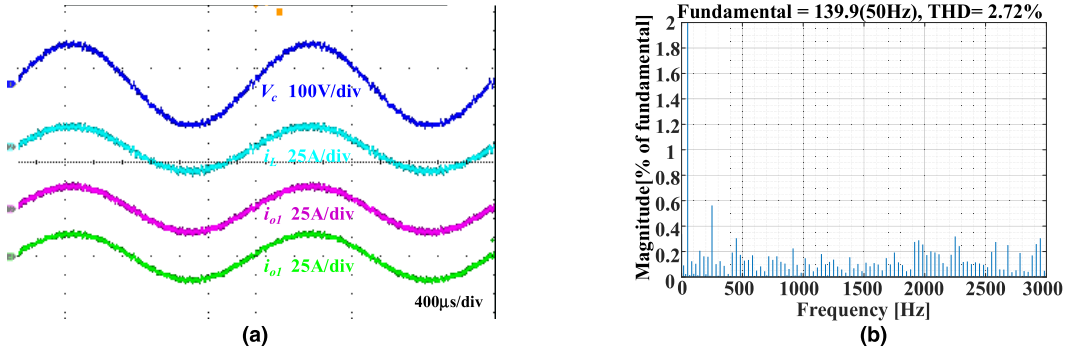

FIGURE 13. Steady-state waveforms (a) and THD (b) of hierarchical linear control.

sented. The proposed scheme has a smaller THD (2.71%) than the typical one (4.26%). The main cause for the improvement is the predictive horizon is set as two, which compensates for the calculation delay in actuation. Fig. 12 depicts the steady-state performance of two-step FSC-MPC without the usage of the current estimator, whose THD is slightly lower than the proposed method. Considering that one current sensor is reduced, small degradation in steady-state performance is acceptable. Fig. 13 shows the result of hierarchical linear control, where conventional droop control with inner double feedback loops is used to control the VSIs. In comparison, the proposed control scheme offers comparable THD with hierarchical linear control. However, the hierarchical control scheme has a larger tracking error than the proposed scheme as Fig. 13 illustrates an observable lower fundamental voltage. It proves that proposed scheme has better fundamental voltage tracking performance than hierarchical linear control. This is because the complicated feedback loops that cause tracking error are avoided.

The transient real-time simulation is performed to examine the transient recovery time and overshoot of the magnitude of current and voltage under connecting and disconnecting process of DGs. In the beginning, only DG1 is connected to the load. Then, DG2 with identical nominal parameters is linked to the system. Fig. 14 and Fig. 15 illustrate the transient responses of proposed scheme and hierarchical linear control, respectively. The output current of DG2 i_{o2} rises from zero to the same value of i_{o1} in the transient stage, which means that both strategies split the load evenly. It can be observed

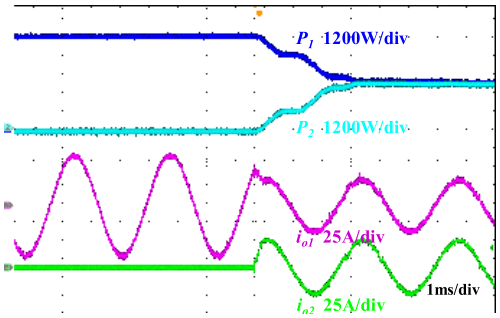

FIGURE 14. Transient performance of proposed scheme.

that the proposed scheme has faster and smoother transient performance, while hierarchical control has excessive overshoot and longer setting time. The comparison of Fig. 14 and Fig. 16 indicates that the current estimator does not influence the transient performance of the system since both have stable and sinusoidal voltage waveforms. Fig. 17 shows the profiles of measured capacitor current and estimated capacitor current from the current observer. The results reveal that the estimated capacitor current by the observer is fairly consistent with that by measurement. This indicates that satisfactory capacitor current estimation can be obtained by using the proposed control scheme.

B. ROBUSTNESS AGAINST MODEL PARAMETER UNCERTAINTY

To investigate the robustness of the proposed method against model parameter uncertainty, the system behavior is tested

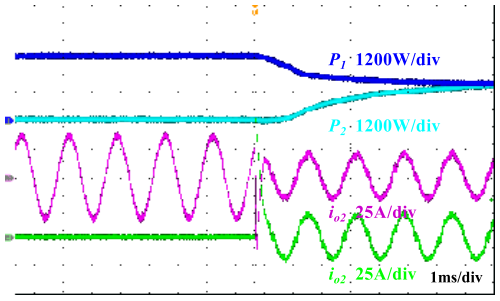

FIGURE 15. Transient performance of hierarchical linear control.

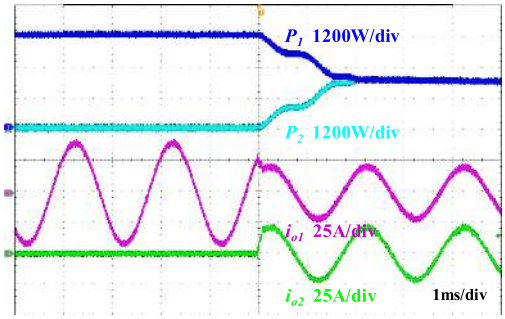

FIGURE 16. Transient performance of two-step FCS MPC.

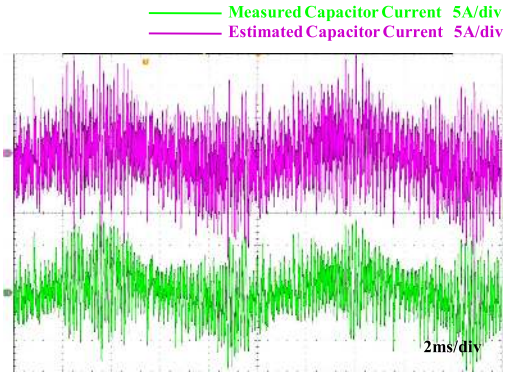

FIGURE 17. Estimated and measured capacitor current.

in MATLAB simulation for a series of different L_f and C_f settings in predictive model. The parameters of the actual inductance and capacitance are chosen as the values indicated in Table 2. Quantitative comparisons of THD and voltage root mean square error (RMSE) between voltage reference and output voltage are illustrated in Table 3. It reflects that the proposed method offers sufficient robustness against parameter uncertainty. The performance deterioration of the proposed control method is small and acceptable in most cases of the model mismatches. Moreover, fundamental voltage tracking error and THD are somewhat more sensitive to inductance variation than capacitor mismatch, especially when the inductance in the predictive model is larger than that in the physical system. It can be seen that algorithm behaves slightly better when it uses somewhat lower capacitance values than the real physical parameter. Nevertheless, it proves that the algorithm is robust against a wide range of parameter mismatch to nominal value. Therefore, precise setting in the model is not of crucial importance.

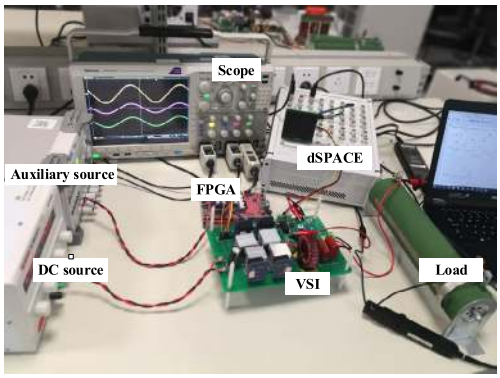

FIGURE 18. Experimental Setup.

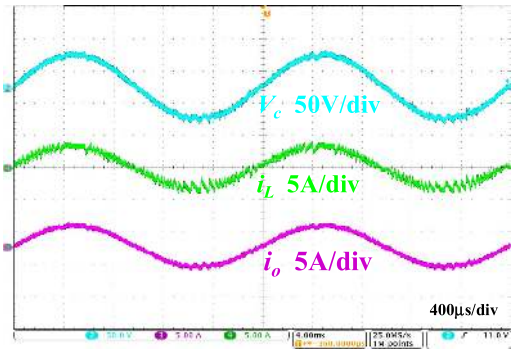

FIGURE 19. Steady-state waveforms of FCS MPC without estimator.

TABLE 3. Sensitivity to model parameter uncertainty of the proposed scheme.

Parameter Uncertainties	Voltage RMSE (V)	THD(%)
L_f and C_f	2.16	2.74
-50%L_f and C_f	4.21	3.52
L_f and -50%C_f	1.96	2.53
+50%L_f and C_f	5.96	3.19
L_f and +50%C_f	2.42	2.88
-50%L_f and -50%C_f	4.61	3.86
+50%L_f and +50%C_f	5.99	3.14

C. EXPERIMENTAL VALIDATION

To verify the concept of improved MPC, a hardware prototype with one VSI is implemented and tested in the laboratory. The hardware platform is shown in Fig. 18. The proposed algorithm and two-step FCS-MPC (without current estimator) are implemented in dSPACE DS1202 to test the influence of observer. It is worth mentioning that FCS-MPC without estimator needs information from two current sensors and a voltage sensor, while the modified FCS-MPC algorithm with the current estimator only needs one voltage sensor. A 100 V DC supply is connected to an LC-filtered inverter feeding a resistive load. The system power rating is 120 W. The inductance and capacitance of LC filter are 2.5mH and 20μF. A Xilinx PYNQ-Z2 FPGA board is employed to generate the gate signals with deadband. Fig. 19 and Fig. 20 shows the comparison of steady-state performance of FSC-MPC with and without the current estimator. The waveforms of

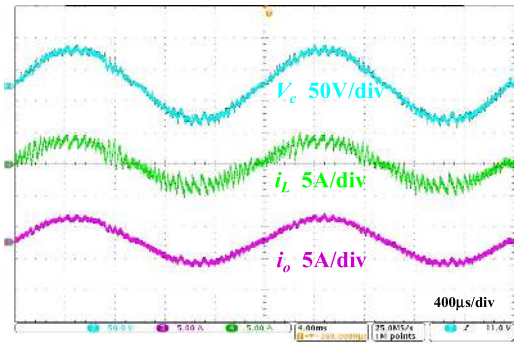

FIGURE 20. Steady-state waveforms of proposed FCS-MPC scheme with estimator.

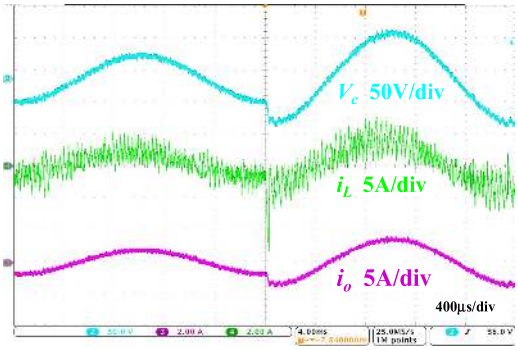

FIGURE 21. Step change performance of FCS MPC without estimator.

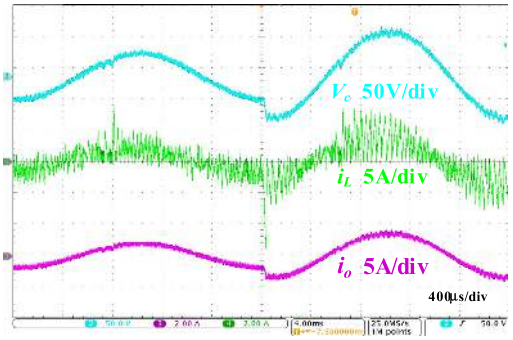

FIGURE 22. Step change performance of proposed FCS-MPC scheme with estimator.

capacitor voltage v_c, inductor current i_L, and load current i_o, are presented. It can be observed that the proposed FSC-MPC has only a slightly larger voltage THD than the case where no observer is used due to the system noise. To test the dynamic performance, a reference voltage step change test is performed. The experimental results are captured in Fig. 21 and Fig. 22. In this experiment, the amplitude of voltage reference changes from 40V to 80V. It reflects that the oscillation caused by the reference step of both methods are similar, revealing a similar robustness against the reference step variations.

VII. CONCLUSION

This article presents an improved two-step FCS-MPC scheme for islanded ac microgrids. The system description of islanded ac microgrid is firstly introduced. To reduce the current sensor of the inductor current in the typical FCS-MPC, the predictive model is reconstructed and a current observer is designed based on capacitor current estimation. Droop control with resistive virtual impedance is used as an outer loop to control the power flow while no bandwidth limitation exists in the proposed scheme. The proposed scheme offers competitive steady-state performance with the hierarchical linear control scheme, whereas the transient performance is dramatically improved. Additionally, the proposed control scheme has the merits of flexible extensibility, low hardware budget, and compact structure. HIL simulation and experimental results are presented to verify the concept.

REFERENCES

[1] H. Han, X. Hou, J. Yang, J. Wu, M. Su, and J. M. Guerrero, "Review of power sharing control strategies for islanding operation of AC microgrids," *IEEE Trans. Smart Grid*, vol. 7, no. 1, pp. 200–215, Jan. 2016.

[2] Y. Karimi, H. Oraee, and J. M. Guerrero, "Decentralized method for load sharing and power management in a hybrid single/three-phase-islanded microgrid consisting of hybrid source PV/Battery units," *IEEE Trans. Power Electron.*, vol. 32, no. 8, pp. 6135–6144, Aug. 2017.

[3] T. Wu, Z. Liu, J. Liu, S. Wang, and Z. You, "A unified virtual power decoupling method for droop-controlled parallel inverters in microgrids," *IEEE Trans. Power Electron.*, vol. 31, no. 8, pp. 5587–5603, Aug. 2016.

[4] L. Sun, G. Wu, Y. Xue, J. Shen, D. Li, and K. Y. Lee, "Coordinated control strategies for fuel cell power plant in a microgrid," *IEEE Trans. Energy Convers.*, vol. 33, no. 1, pp. 1–9, Mar. 2018.

[5] M. Fakhari Moghaddam Arani and Y. A.-R.-I. Mohamed, "Dynamic droop control for wind turbines participating in primary frequency regulation in microgrids," *IEEE Trans. Smart Grid*, vol. 9, no. 6, pp. 5742–5751, Nov. 2018.

[6] M. Lei, Z. Yang, Y. Wang, H. Xu, L. Meng, J. C. Vasquez, and J. M. Guerrero, "An MPC-based ESS control method for PV power smoothing applications," *IEEE Trans. Power Electron.*, vol. 33, no. 3, pp. 2136–2144, Mar. 2017.

[7] X. Hou, Y. Sun, J. Lu, X. Zhang, L. H. Koh, M. Su, and J. M. Guerrero, "Distributed hierarchical control of AC microgrid operating in grid-connected, islanded and their transition modes," *IEEE Access*, vol. 6, pp. 77388–77401, 2018.

[8] C. Zhang, J. M. Guerrero, J. C. Vasquez, and E. A. A. Coelho, "Control Architecture for Parallel-Connected Inverters in Uninterruptible Power Systems," *IEEE Trans. Power Electron.*, vol. 31, no. 7, pp. 5176–5188, Sep. 2016.

[9] J. M. Guerrero, L. GarciadeVicuna, J. Matas, M. Castilla, and J. Miret, "A wireless controller to enhance dynamic performance of parallel inverters in distributed generation systems," *IEEE Trans. Power Electron.*, vol. 19, no. 5, pp. 1205–1213, Sep. 2004.

[10] H. Mahmood, D. Michaelson, and J. Jiang, "Accurate reactive power sharing in an islanded microgrid using adaptive virtual impedances," *IEEE Trans. Power Electron.*, vol. 30, no. 3, pp. 1605–1617, Mar. 2015.

[11] A. Milczarek, M. Malinowski, and J. M. Guerrero, "Reactive power management in islanded microgrid—Proportional power sharing in hierarchical droop control," *IEEE Trans. Smart Grid*, vol. 6, no. 4, pp. 1631–1638, Jul. 2015.

[12] Q.-C. Zhong, Y. Wang, and B. Ren, "UDE-based robust droop control of inverters in parallel operation," *IEEE Trans. Ind. Electron.*, vol. 64, no. 9, pp. 7552–7562, Sep. 2017.

[13] Q.-C. Zhong and Y. Zeng, "Universal droop control of inverters with different types of output impedance," *IEEE Access*, vol. 4, pp. 702–712, 2016.

[14] Z. Li, C. Zang, P. Zeng, H. Yu, and S. Li, "Fully distributed hierarchical control of parallel grid-supporting inverters in islanded AC microgrids," *IEEE Trans Ind. Informat.*, vol. 14, no. 2, pp. 679–690, Feb. 2018.

[15] Y. Han, H. Li, P. Shen, E. A. A. Coelho, and J. M. Guerrero, "Review of active and reactive power sharing strategies in hierarchical controlled microgrids," *IEEE Trans. Power Electron.*, vol. 32, no. 3, pp. 2427–2451, Mar. 2017.

[16] J. M. Guerrero, M. Chandorkar, T. L. Lee, and P. C. Loh, "Advanced control architectures for intelligent microgrids—Part I: Decentralized and hierarchical control," *IEEE Trans. Ind. Electron.*, vol. 60, no. 4, pp. 1254–1262, Apr. 2013.

[17] P. Cortés, M. P. Kazmierkowski, R. M. Kennel, D. E. Quevedo, and J. Rodriguez, "Predictive control in power electronics and drives," *IEEE Trans. Ind. Electron.*, vol. 55, no. 12, pp. 4312–4324, Oct. 2008.
[18] T. John, Y. Wang, K. T. Tan, and P. L. So, "Coordinated operation of a microgrid with a distribution network device," in *Proc. IEEE Innov. Smart Grid Technol.-Asia (ISGT ASIA)*, Nov. 2016, pp. 1–6.
[19] P. Cortés, G. Ortiz, J. I. Yuz, J. Rodríguez, S. Vazquez, and L. G. Franquelo, "Model predictive control of an inverter with output *LC* filter for UPS applications," *IEEE Trans. Ind. Electron.*, vol. 56, no. 6, pp. 1875–1883, Jun. 2009.
[20] C. Zheng, T. Dragicevic, and F. Blaabjerg, "Current-sensorless finite-set model predictive control for LC-filtered voltage source inverters," *IEEE Trans. Power Electron.*, vol. 35, no. 1, pp. 1086–1095, Jan. 2020.
[21] C. Zheng, T. Dragicevic, B. Majmunovic, and F. Blaabjerg, "Constrained modulated model-predictive control of an *LC*-filtered voltage-source converter," *IEEE Trans. Power Electron.*, vol. 35, no. 2, pp. 1967–1977, May 2020.
[22] S. Vazquez, J. I. Leon, L. G. Franquelo, J. Rodriguez, H. A. Young, A. Marquez, and P. Zanchetta, "Model predictive control: A review of its applications in power electronics," *IEEE Ind. Electron. Mag.*, vol. 8, no. 1, pp. 16–31, Mar. 2014.
[23] J. Rodriguez, M. P. Kazmierkowski, J. R. Espinoza, P. Zanchetta, H. Abu-Rub, H. A. Young, and C. A. Rojas, "State of the art of finite control set model predictive control in power electronics," *IEEE Trans Ind. Informat.*, vol. 9, no. 2, pp. 1003–1016, May 2013.
[24] T. Geyer and D. E. Quevedo, "Performance of multistep finite control set model predictive control for power electronics," *IEEE Trans. Power Electron.*, vol. 30, no. 3, pp. 1633–1644, Mar. 2014.
[25] S. Mukherjee, P. Shamsi, and M. Ferdowsi, "Control of a single-phase standalone inverter without an output voltage sensor," *IEEE Trans. Power Electron.*, vol. 32, no. 7, pp. 5601–5612, Jul. 2017.
[26] G. Lou, W. Gu, Y. Xu, M. Cheng, and W. Liu, "Distributed MPC-based secondary voltage control scheme for autonomous droop-controlled microgrids," *IEEE Trans. Sustain. Energy*, vol. 8, no. 2, pp. 792–804, Apr. 2017.
[27] K.-S. Low and R. Cao, "Model predictive control of parallel-connected inverters for uninterruptible power supplies," *IEEE Trans. Ind. Electron.*, vol. 55, no. 8, pp. 2884–2893, Aug. 2008.
[28] K. T. Tan, X. Y. Peng, P. L. So, Y. C. Chu, and M. Z. Q. Chen, "Centralized control for parallel operation of distributed generation inverters in microgrids," *IEEE Trans. Smart Grid*, vol. 3, no. 4, pp. 1977–1987, Dec. 2012.
[29] T. Dragicevic, "Model predictive control of power converters for robust and fast operation of AC microgrids," *IEEE Trans. Power Electron.*, vol. 33, no. 7, pp. 6304–6317, Jul. 2018.
[30] Y. Shan, J. Hu, Z. Li, and J. M. Guerrero, "A model predictive control for renewable energy based AC microgrids without any PID regulators," *IEEE Trans. Power Electron.*, vol. 33, no. 11, pp. 9122–9126, Nov. 2018.
[31] P. Cortés, J. Rodríguez, D. Quevedo, and C. Silva, "Predictive current control strategy with imposed load current spectrum," in *Proc. 12th Int. Power Electron. Motion Control Conf. (EPE-PEMC)*, 2007, pp. 252–257.
[32] P. Cortes, J. Rodriguez, C. Silva, and A. Flores, "Delay compensation in model predictive current control of a three-phase inverter," *IEEE Trans. Ind. Electron.*, vol. 59, no. 2, pp. 1323–1325, Feb. 2012.
[33] C. Zhang, J. M. Guerrero, J. C. Vasquez, E. A. Coelho, and C. Seniger, "High-performance control of paralleled three-phase inverters for residential microgrid architectures based on online uninterruptable power systems," in *Proc. IEEE Appl. Power Electron. Conf. Expo. (APEC)*, Mar. 2015, pp. 3232–3239.
[34] D. Rowell, "Discrete time observers and LQG control," Dept. Mech. Eng., Massachusetts Inst. Technol., Cambridge, MA, USA, Lecture Notes, 2004, vol. 1, no. 3.
[35] X. Wang, Y. W. Li, F. Blaabjerg, and P. C. Loh, "Virtual-impedance-based control for voltage-source and current-source converters," *IEEE Trans. Power Electron.*, vol. 30, no. 12, pp. 7019–7037, Dec. 2015.
[36] W. Yao, M. Chen, J. Matas, J. M. Guerrero, and Z.-M. Qian, "Design and analysis of the droop control method for parallel inverters considering the impact of the complex impedance on the power sharing," *IEEE Trans. Ind. Electron.*, vol. 58, no. 2, pp. 576–588, Feb. 2011.
[37] T. Dragicevic and M. Novak, "Weighting factor design in model predictive control of power electronic converters: An artificial neural network approach," *IEEE Trans. Ind. Electron.*, vol. 66, no. 11, pp. 8870–8880, Nov. 2019.

TIANHAO CHEN (Student Member, IEEE) was born in China, in 1995. He received the B.S. degree in automation from Southeast University, Nanjing, China, in 2017. He is currently pursuing the M.S. degree in power electronics with ShanghaiTech University, Shanghai, China. He has been a Graduate Research Assistant with the Power Electronics and Renewable Energies Laboratory, ShanghaiTech University. His current research interests include power electronics, microgrids, and model predictive control.

OMAR ABDEL-RAHIM (Senior Member, IEEE) received the bachelor's and master's degrees in electrical engineering from the Faculty of Engineering, Aswan University, Aswan, Egypt, in 2009 and 2012, respectively, and the Ph.D. degree from Utsunomiya University, Japan, in 2017. He is currently a Postdoctoral Fellow of the School of Information Science and Technology, ShanghaiTech University, China. Since October 2017, he has been an Assistant Professor with the Faculty of Engineering, Aswan University. From 2009 to 2012, he was a Research Assistant with the Aswan Power Electronic Application Research Center (APEARC). Since 2010, he has been with Aswan University, where he was an Assistant Lecturer with the Department of Electrical Engineering, Aswan Faculty of Engineering. In 2012, he joined Texas A&M University, Qatar, as a Research Associate. He has authored or coauthored over 30 articles in leading international conferences and journals, mainly on the topics of grid connected inverters and multiphase matrix converters. His current research interests include multiphase machines drives, predictive control, renewable energy, and smart grid and dc–ac converters.

FAXIANG PENG (Student Member, IEEE) received the B.S. degree in electrical engineering and automation from the Xi'an University of Technology (XUT), Xi'an, China, in 2017. He is currently pursuing the M.S. degree with the School of Information Science and Technology, ShanghaiTech University, Shanghai, China.

His research interests include battery management systems and resonant converter design. He was nominated as the Finalist of the IEEE IAS TSC Prize Paper Award, in 2019, for his first-authored paper.

HAOYU WANG (Senior Member, IEEE) received the bachelor's degree (Hons.) in electrical engineering from Zhejiang University, Hangzhou, China, and the Ph.D. degree in electrical engineering from the University of Maryland, College Park, MD, USA.

He is currently a tenure track Assistant Professor with the School of Information Science and Technology, ShanghaiTech University, Shanghai, China. His research interests include power electronics, plug-in electric and hybrid electric vehicles, the applications of wide bandgap semiconductors, renewable energy harvesting, and power management integrated circuits.

Dr. Wang is an Associate Editor of the IEEE TRANSACTIONS ON TRANSPORTATION ELECTRIFICATION and *CPSS Transactions on Power Electronics and Applications*.